

Experimental quantum secure network with digital signatures and encryption

Hua-Lei Yin,^{1,*} Yao Fu,^{2,†} Chen-Long Li,^{1,2} Chen-Xun Weng,^{1,2} Bing-Hong Li,^{1,2} Jie Gu,¹ Yu-Shuo Lu,¹ Shan Huang,¹ and Zeng-Bing Chen^{1,2,‡}

¹*National Laboratory of Solid State Microstructures, School of Physics, Collaborative Innovation Center of Advanced Microstructures, Nanjing University, Nanjing 210093, China*
²*MatricTime Digital Technology Co. Ltd., Nanjing 211899, China*

Cryptography promises four information security objectives, namely, confidentiality, integrity, authenticity and nonrepudiation, to support trillions of transactions every year in the digital economy. Efficient digital signatures, ensuring the integrity, authenticity and nonrepudiation of data with provable security, are highly urgent and intractable open problems. Here, we propose a protocol of high-efficiency quantum digital signature using secret sharing, one-time universal₂ hashing and the one-time pad. We just need to use a 384-bit key to sign documents of up to 2^{64} lengths with a security bound of 10^{-19} . If one megabit document is signed, the signature efficiency is improved by more than 10^8 times compared with previous quantum digital signature protocols. Furthermore, we build the first all-in-one quantum secure network integrating provably secure communication, digital signatures, secret sharing and conference key agreement and experimentally demonstrate this signature efficiency advantage. Our work completes the cryptography toolbox of the four information security objectives.

I. INTRODUCTION

Fast developing driverless, blockchain and artificial intelligence technology, as well as digital currency systems, will soon require a more robust network with security against quantum attacks [1]. A promising blueprint for such a network ensures one-way hash functions, encryption algorithms and digital signatures with information-theoretical security, which cannot be met in the current Internet with public-key infrastructure [2]. Currently, the widely implemented one-way hash functions Message Digest-5 [3] and Secure Hash Algorithm-1 [4] are no longer secure. For example, one can utilize two different files to obtain the identical hash value after carrying out Secure Hash Algorithm-1 since 2017 [5]. In addition, the public-key (or asymmetric-key) encryption algorithms [6–8], based on the computational complexity of factorization [9] and discrete logarithm [10], have both been compromised at the 795-bit level in 2020 [8]. More seriously, quantum computers can in principle attack public-key cryptosystems with any number of bits [11].

Different from public-key cryptography, one-time pad (OTP) encryption based on a symmetric key provides a way of transmitting a message with provable confidentiality [12] over a standard communication channel, where the symmetric key is securely established using quantum key distribution [13] with no restriction on the computational power of attackers. Currently, experimental demonstrations and commercial applications of quantum key distribution have arisen widely around the world [14–16].

The provable security possessed by quantum key dis-

tribution [13] and quantum secure direct communication [17, 18] only ensures confidentiality, which is, however, an incomplete solution to the remaining cryptographic tasks. Three other fundamental information security objectives are data integrity, data origin authentication and nonrepudiation [2], which are usually realized in classical cryptosystems by digital signatures using one-way hash functions and public-key encryption algorithms, as shown in Fig. 1a. Digital signatures [2] play a vital role in software distributions, e-mails, web browsing and financial transactions, but become insecure as one-way hash functions and public-key encryption algorithms used therein are breakable by either classical or quantum computers [19].

Different from classical solutions [9, 10], quantum digital signatures (QDS) promise to sign a document with provable integrity, authenticity and nonrepudiation via quantum laws. The first rudiment of the QDS was introduced in 2001 [20], but it cannot be implemented due to some impractical requirements. Recent developments have removed impractical requirements such as high-dimensional single-photon state [21], quantum memory [22] and secure quantum channels [23–26] and thus enable demonstrations of QDS in various experimental systems [27–32]. The resulting schemes still have serious limitations that require an approximately 10^5 -bit key to sign only a one-bit message. The best signature rate reported thus far is less than 1 time per second (tps) for a one-bit message at 100 km transmission distance for a gigahertz system [31]. Additionally, one cannot know how to efficiently sign multibit messages with provable security [33], which makes all known single-bit-type QDS protocols impractical [20–32]. Thus, a QDS with both high efficiency and unconditional security is highly desired and is an intractable open problem. Note that using entanglement correlation, a probabilistic one-time delegation of signature authority protocol is proposed and demonstrated [34].

*Electronic address: hlyin@nju.edu.cn

†Electronic address: yaofu@mail.ustc.edu.cn

‡Electronic address: zbchen@nju.edu.cn

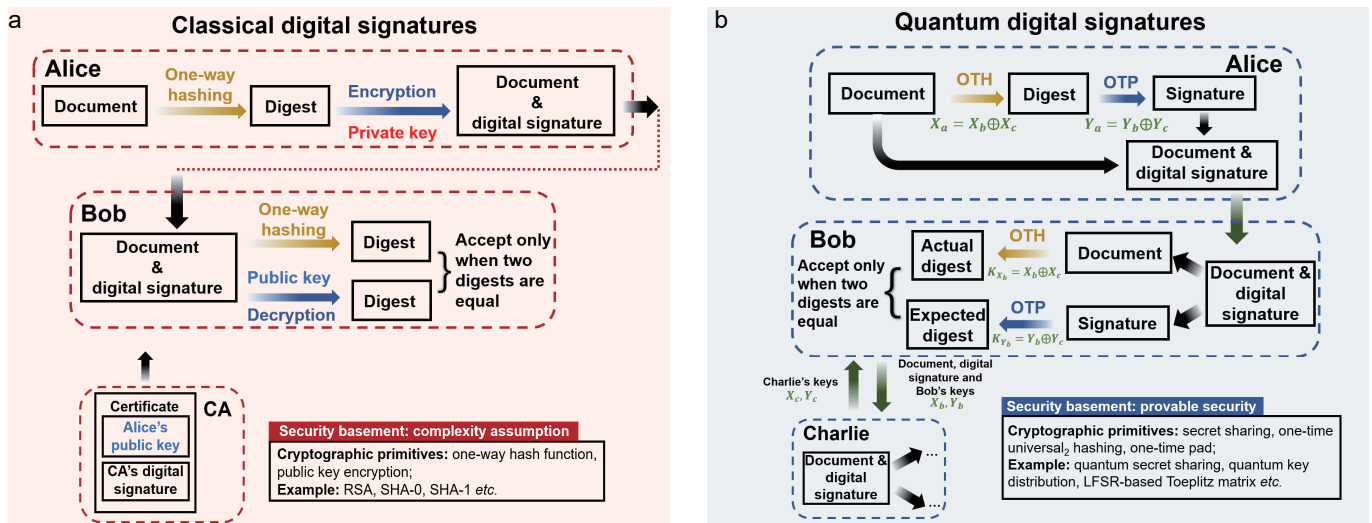


FIG. 1: Schematic diagram for classical and quantum digital signatures. (a) Classic scheme with a one-way hash function and public-key encryption. Alice encrypts the digest to obtain the signature by a private key, where the digest is acquired via a fixed one-way hash function. She sends the document along with the signature to Bob, who utilizes the same one-way hash function and the corresponding public key to acquire two digests. Then, Bob accepts the signature if two digests are identical. Thereinto, a digital certificate issued by the certificate authority (CA) guarantees the validity of the public key. The security of classical digital signatures is based on the computational complexity assumption. Cryptographic primitives based on such assumptions include one-way hash functions and public key encryption, such as SHA-0, SHA-1, RSA, etc. (b) Our quantum digital signatures scheme with secret sharing, one-time universal₂ hashing (OTH) and one-time pad (OTP), where secret sharing can guarantee unconditional security via quantum laws. Compared with the classical scheme, Charlie plays the role of CA, Alice’s key can be seen as a private key, while Bob’s key is a public key—they are asymmetric in our QDS protocol. The secret sharing, OTH and OTP all have provable security. Our quantum digital signatures scheme has provable security. To generate keys required by our quantum digital signature protocol, quantum secret sharing and quantum key distribution protocols can be used.

Here, we propose an entirely different QDS protocol capable of signing an arbitrarily long document with unconditional security. For example, just with a 384-bit key, we can sign documents of up to 2^{64} lengths with a security bound of 10^{-19} . For the first time, we propose the concept of one-time universal₂ hashing (OTH), i.e., the universal₂ hash function used for each digital signature is completely random. Our protocol not only uses OTH and OTP as the underlying cryptography layer but also uses secret sharing to realize perfect bits correlation of three parties, then building an asymmetric key relationship for Alice and Bob. Secret sharing can be implemented with provable security by using quantum secret sharing, quantum key distribution or future quantum internet with solid-state entanglement. We simulate the performances of our QDS protocol based on a variety of quantum communication protocols. The simulation results show that the signature rates are more than 10^4 tps in the metropolitan area if we use a gigahertz system, which represents an efficiency improvement of at least eight orders of magnitude for signing one megabit document. We also experimentally construct a trusted-repeater quantum secure network to realistically demonstrate cryptographic primitives [2] with information-theoretical security, including private com-

munication, digital signatures, secret sharing and conference key agreement. In our experiment, the signature efficiency can be achieved 1.43×10^8 times of the previous work in Ref. [24] considering the improvements in signature rates for signing a 130,250 bytes document over 101 km fiber and the security bound is as small as 10^{-32} , which shows a significant advantage.

II. EFFICIENT QDS PROTOCOL

Our proposal utilizes secret sharing, OTH and OTP to generate and verify signatures, as shown in Fig. 1b. Let Alice be the signer and Bob and Charlie be the receiver. Before executing the signature, all of them have two sets of keys, $X_{a,b,c}$ and $Y_{a,b,c}$, which satisfy the bit correlations $X_a = X_b \oplus X_c$ (n bits) and $Y_a = Y_b \oplus Y_c$ ($2n$ bits). The perfect bit correlation of three parties can be realized by using quantum communication, such as quantum secret sharing and quantum key distribution. Suppose that Alice signs an m -bit document (message), denoted as Mes , to the desired recipient, Bob.

(i) *Signing*—Alice randomly generates an irreducible polynomial [2] $p(x)$ of degree n by using a local quantum random number, which can be characterized by an

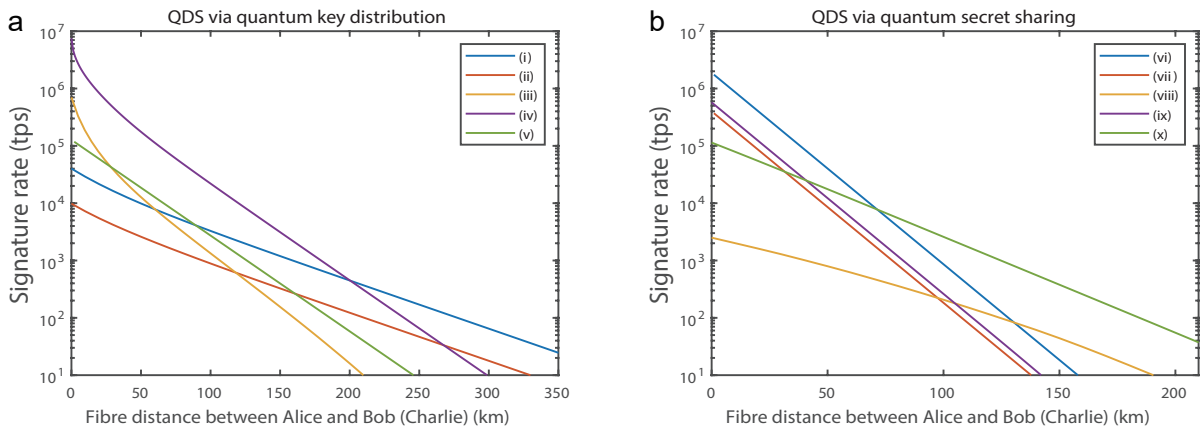


FIG. 2: Signature rates versus fiber distances. (a) The rate via quantum key distribution. (b) The rate via quantum secret sharing. Lines labeled (i)-(v) represent sending-or-not-sending twin-field [35] (i), phase-matching [36] (ii), discrete-modulated continuous-variable [37] (iii), Gaussian-modulated continuous-variable [38] (iv) and measurement-device-independent [39] (v) quantum key distribution protocols. Lines labeled (vi)-(x) represent prepare-and-measure [40] (vi), measurement-device-independent [41] (vii), round-robin [42] (viii), single-qubit [43] (ix) and differential-phase-shift [44] (x) quantum secret sharing protocols. To simplify, let the channel loss of Alice-Bob and Alice-Charlie be the same. We need a 384-bit key for performing each digital signature with a security bound of approximately 1.1×10^{-19} for documents of up to 2^{64} length. The signature rates are more than 10^4 tps in the metropolitan area if we use a gigahertz system.

n -bit string p_a (see Supplementary Information). Then she uses her key bit string X_a and the irreducible polynomial $p(x)$ to generate a random linear feedback shift register-based (LFSR-based) Toeplitz matrix [45] H_{nm} with n rows and m columns. She acquires a $2n$ -bit digest $Dig = (Dig_1 || p_a)$. Here, Dig_1 is the digest of the m -bit document through a hash operation with $Dig_1 = H_{nm} \cdot Mes$, and p_a is an n -bit string for generating the irreducible polynomial in the LFSR-based Toeplitz matrix. Then, Alice encrypts the digest with her key bit string Y_a to obtain the $2n$ -bit signature $Sig = Dig \oplus Y_a$. She sends the document and signature $\{Sig, Mes\}$ to Bob.

(ii) *Verification of Bob*—Bob transmits $\{Sig, Mes\}$ as well as his key bit strings $\{X_b, Y_b\}$ to Charlie to inform Charlie that he has received the signature. Then, Charlie forwards his key bit strings $\{X_c, Y_c\}$ to Bob. Bob obtains two new key bit strings $\{K_{X_b} = X_b \oplus X_c, K_{Y_b} = Y_b \oplus Y_c\}$ by the XOR operation. He exploits K_{Y_b} to obtain an expected digest and a string p_b via XOR decryption. He utilizes K_{X_b} and p_b to establish an LFSR-based Toeplitz matrix and acquires an actual digest via a hash operation. Bob will accept the signature if the actual digest is equal to the expected digest. Then, he informs Charlie of the result.

(iii) *Verification of Charlie*—If Bob announces that he accepts the signature, Charlie creates two new key bit strings $\{K_{X_c} = X_b \oplus X_c, K_{Y_c} = Y_b \oplus Y_c\}$ using his original key and the key sent by Bob. He employs K_{Y_c} to acquire an expected digest and a variable p_c via XOR decryption. Charlie obtains an actual digest via a hash operation, where the hash function is an LFSR-based Toeplitz matrix generated by K_{X_c} and p_c . Charlie ac-

cepts the signature if the two digests are identical.

Note that if Alice, Bob and Charlie are all truthful, there are the relations $p_a = p_b = p_c$ and $X_a = K_{X_b} = K_{X_c}$. Thus, they will use the same universal₂ hash function and generate the same actual digest. The signature will be accepted naturally. One-time pad encryption [12] guarantees the digest with perfect privacy and hides all information about Toeplitz hashing before Bob's decryption. The one-time universal₂ hash function, specifically the random LFSR-based Toeplitz matrix [45], ensures that the used hash function is completely random each time. In this way, Bob's probability of finding any two different documents with the same hash value is $m/(2^{n-1})$, which is practically an ignorable probability (details can be found in Supplementary Information). An authenticated classical channel [45, 46] between Bob and Charlie, implemented by LFSR-based Toeplitz hashing and one-time pad encryption, is used to ensure that the corresponding new key bit strings of Bob and Charlie are the same. Once Bob accepts the signature, Charlie definitely accepts it. Thus, the security bound of our QDS is less than $2^{64}/(2^{128-1}) \approx 1.1 \times 10^{-19}$ for documents of up to 2^{64} lengths if one uses a 128-bit key for hashing and another 256-bit key for encryption.

III. SIMULATION RESULTS

Secret sharing allows the key strings of Alice, Bob and Charlie to satisfy $K_a = K_b \oplus K_c$ with $K \in \{X, Y\}$, which can be implemented with provable security by using quantum secret sharing [41], quantum key distribution [13] or future quantum internet with solid-state en-

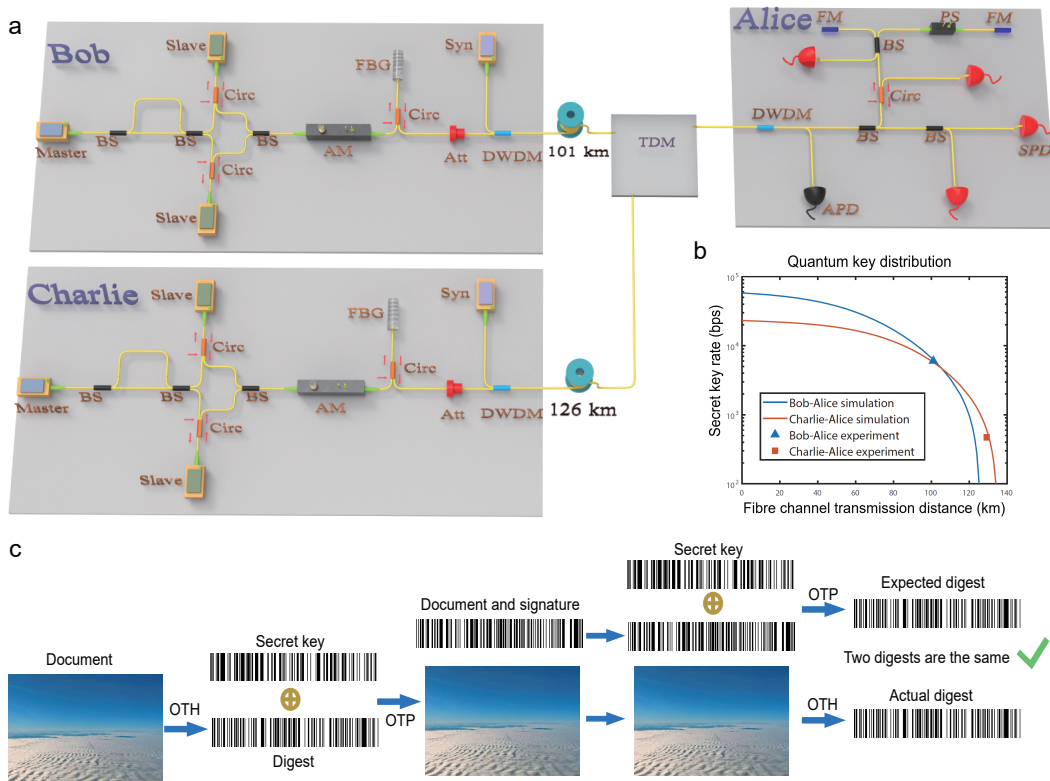


FIG. 3: Experimental setup of the quantum secure network. (a) Bob (Charlie) exploits a master laser, an asymmetric interferometer, two slave lasers, two circulators (Circ) and a beam splitter (BS) to prepare optical pulses in the Z and X bases by controlling the trigger electrical signal of slave lasers. The decoy signals are generated by the amplitude modulator (AM), while the vacuum state is produced by removing the triggered signal of slave lasers. The optical pulses pass through a set of fiber Bragg grating (FBG), circulator and attenuator (Att) to be modulated at the single-photon level. The synchronization (Syn) signal is transmitted with a dense wavelength division multiplexer (DWDM) to quantum channels. The synchronization pulse is detected by an avalanche photodiode (APD). A biased beam splitter is utilized for realizing a passive basis measurement with single-photon detector (SPD). Two Faraday mirrors (FM), a phase shifter (PS) and a beam splitter form an asymmetric interferometer. The quantum signals sent by Bob (Charlie) arrive at Alice by time division multiplexing (TDM). (b) Experimental results of the decoy-state quantum key distribution. The blue and red curves of the secret key rate correspond to the simulation results using experimental parameters. (c) Demonstration of quantum digital signatures. The document to be signed with a length of 130,250 bytes includes the timestamp, identity number of the desert image and the image itself.

tanglement. While a full-blown quantum internet [47], with functional quantum computers and quantum repeaters as nodes connected through quantum channels, is still on the way, the first prototype of quantum internet has been realized with remote solid-state qubits [48] in multiparty entanglement applicable to secret sharing. To date, there is no workable quantum-secure asymmetric cryptosystem. With the help of secret sharing, our framework represents the first practical quantum asymmetric cryptosystem immediately applicable to secure digital signatures. Here we simulate the performances of our QDS protocol using various quantum key distribution [35–39] and quantum secret sharing [40–44] protocols (see Supplementary Information), as depicted in Fig. 5. For a gigahertz system and the symmetric channel case, the simulation results show that one can implement digital signatures up to 10^4 tps even for the 2^{64} -bit document if the fiber distance between Alice and Bob

(Charlie) is less than 50 kilometers. Therefore, it is possible to conduct tens of thousands of transactions per second secured by digital signatures in the metropolitan area network [16].

Our QDS protocol has two significant features. The first is that as the length of the signed document increases up to 10^{19} bits, the key bits (secret sharing) consumed by our QDS protocol are almost constant, while having sufficient security as discussed above. This means that the signature efficiency of our protocol has a significant advantage over previous single-bit-type QDS protocols [20–32]. As the length of the document is increased from 1 to 10^{19} bits, our quantum resource consumption (384-bit key) does not change, which means that the signature time will not increase. Thereby, our protocol has the signature efficiency advantage from 10^2 to 10^{21} , since previous protocols need at least 10^5 bits to sign one bit [28–32]. The second feature is that our QDS protocol is flexible for

TABLE I: List of the experimental results of the QDS in Ref. [24] and our QDS protocol. At each time, a document of 10^6 bits is assumed to be signed.

	Ref. [24]	our protocol
distance between Bob and Charlie (km)	101+126=227	101+126=227
keys consumption (bit)	1.09×10^{12} (4.66×10^{11})	384
valid keys length per second (bit)	9314	470
signature rate (tps)	8.54×10^{-9} (2.00×10^{-8})	1.22
security bound (ϵ)	10^{-32} (10^{-10})	10^{-32}

applications. All known and future developed quantum secret sharing and quantum key distribution protocols can be used for perfect bits correlation of three parties (secret sharing) in our QDS. In addition, the universal₂ hash function should not be restricted to be the LFSR-based Toeplitz matrix [45], which is used here just as an example.

IV. EXPERIMENTAL RESULTS

To prove that our QDS protocol is very efficient and practical, we establish a three-node quantum secure network (see Fig. 3a) containing two end nodes (Bob and Charlie) and a repeater node (Alice). Two point-to-point quantum key distribution links are built between Alice-Bob and Alice-Charlie using the decoy-state protocol with a time-bin phase encoding system [49]. Bob (Charlie) multiplexes the 1570-nm synchronization pulse with a 1550-nm quantum signal by a dense wavelength division multiplexer, transmitted through a 101 km (126 km) single-mode optical fiber to Alice; the corresponding loss of quantum channels is 19 (24.3) dB, and the system clock frequency is 200 MHz. To reduce the insertion loss of the receiving end, we take advantage of time division multiplexing by manually switching fiber links. A classic network is used to communicate in the postprocessing stage, including parameter estimation, error correction and privacy amplification (details can be found in the Supplementary Information).

In Fig. 3b, the blue (red) symbol refers to the experimental secret key rates of quantum key distribution between Bob-Alice (Charlie-Alice) with 6021 (470) bits per second by considering the finite-size effects, fitting well with our simulation curves. The blue and red curves are both flattened in the short distance since we introduce dead times of 10 and 25 μ s for the gated-mode InGaAs/InP single-photon detector, respectively.

Here, we describe the experimental demonstration of quantum digital signatures for a $130,250$ byte (1.042×10^6 bits) document over 101 km fiber, as shown in Fig. 3c. The secret sharing is realized in the way that Alice performs an XOR operation for her two key bit strings. One key bit string is shared with Bob by using the time-bin phase encoding quantum key distribution, and the other is generated with Charlie by exploiting another quantum

key distribution system. The signed document includes the timestamp, identity number of the desert image and the image itself. The digest is composed of the 128-bit hash value generated through OTH and the 128-bit irreducible polynomial and is then encrypted to form a signature by OTP. Both the digest and signature are displayed as bar codes and have the same size of 32 bytes (256 bits). The actual and expected digests are identical, which indicates that we have applied successful quantum digital signatures with information-theoretical security.

For a fair comparison, we also demonstrate the QDS of Ref. [24] using the same experimental system, and the results are shown in Table I. The length of the raw key using the method in Ref. [24] (without error correction and privacy amplification) is 2.88×10^6 bits for signing a single-bit message. For a multibit message, for example, one megabit, it requires at least the length of the key with 2.88×10^{12} bits [28, 33]. Therefore, the signature rate of our QDS protocol is 1.22 tps, while using the method of Ref. [24] is only 3.23×10^{-9} tps if we let the size of each signed document be 10^6 bits. For the experimental demonstration of the QDS in Fig. 3c, we only require less than one second to run the quantum secure network, while Ref. [24] will take approximately as long as four years to accumulate data.

To demonstrate the full-function information security objectives, in Fig. 4, we demonstrate the other three cryptographic tasks in our quantum secure network with information-theoretical security, including encryption, secret sharing and conference key agreement. In Fig. 4a, we realize the OTP encryption with the help of Alice as a trust relay. Alice performs an XOR operation for her two key bit strings that are shared with Bob and Charlie. To realize secure encryption between Bob and Charlie, Alice announces the XOR result as a key relay to make Bob and Charlie share identical keys. A prairie image with 112,500 bytes is encrypted via OTP to realize the perfectly private communication. The secret sharing of an image of a mountain with 79,800 bytes has been implemented in Fig. 4b. The XOR result as the key bit string of Alice is only known by herself before the implementation of secure secret sharing. For conference key agreement, Alice, Bob and Charlie can obtain the same key with provable security if the XOR result of Alice is published. An image of a lake with a size of 139,500 bytes is adopted to implement group encryption, as shown in

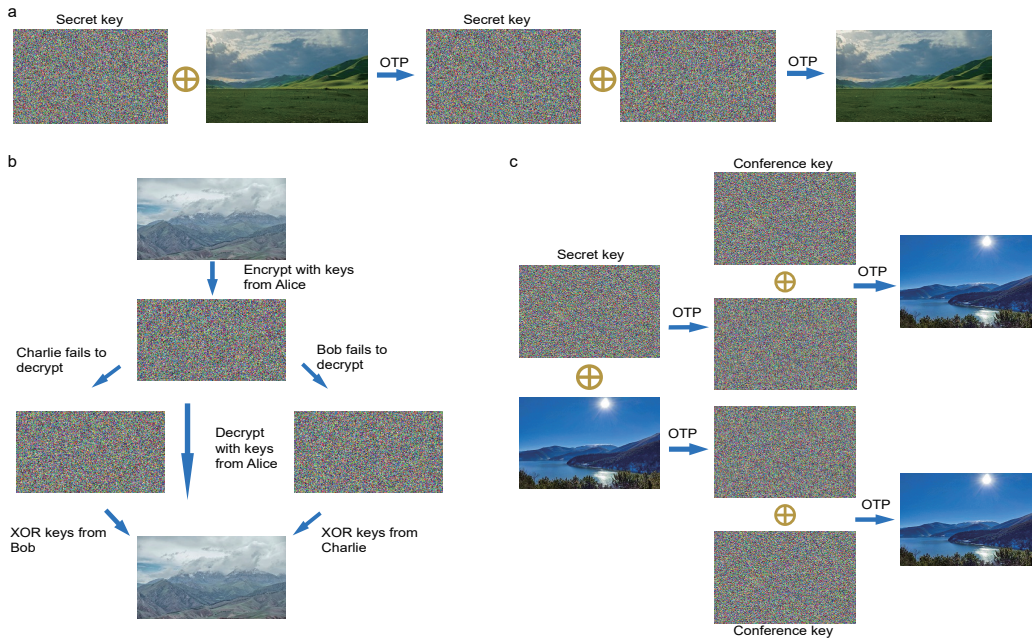


FIG. 4: Experimental demonstration of other cryptographic tasks. All encrypted images and secret (conference) keys are demonstrated as images of white noise. (a) Encryption. A prairie image with 112,500 bytes is encrypted via an OTP, utilizing identical secret keys shared between Bob and Charlie, to realize the perfectly private communication. (b) Secret sharing. An image of a mountain with a size of 79,800 bytes is used to realize provable secret sharing. Only when two users Bob and Charlie work together to reconstruct the secret keys of Alice can they decrypt the image. (c) Conference key agreement. An image of a lake with a size of 139,500 bytes is adopted to implement group encryption. All users of this group can obtain the information of the encrypted figure separately.

Fig. 4c. The cryptographic tasks feature high efficiency and unconditional security on our quantum secure network using the current quantum technology.

V. CONCLUSIONS

In conclusion, we have successfully demonstrated a full-function quantum secure network with all information security objectives, namely, confidentiality, integrity, authenticity and nonrepudiation. In particular, we theoretically propose and experimentally implement a QDS protocol that shows a 100 million-fold signature efficiency improvement. As such, digital signatures, which are of central importance in internet-based digital processing systems, are now promoted to be unconditionally secure and commercially applicable by OTP, OTH and secret sharing. Our framework consumes few resources to sign an almost arbitrarily long document, surpassing all previous protocols not only in signing efficiency but also in security. The full-function quantum secure network can of course be implemented by more advanced technology,

e.g., by a future quantum internet. Its successful implementation by a practical quantum secure network under current technology, as we show above, lays a firm foundation for a quantum secure layer of the current internet. Such a quantum secure internet, enabling main secure cryptographic tasks simultaneously, paves the way for the quantum age of the digital economy.

Acknowledgments

We gratefully acknowledge the support from the Natural Science Foundation of Jiangsu Province (No. BK20211145), the Fundamental Research Funds for the Central Universities (No. 020414380182), the Key Research and Development Program of Nanjing Jiangbei New Area (No. ZDYD20210101), the Program for Innovative Talents and Entrepreneurs in Jiangsu (No. JSSCRC2021484), and the Key-Area Research and Development Program of Guangdong Province (No. 2020B0303040001).

Supplementary Information for Experimental quantum secure network with digital signatures and encryption

1. Cryptography toolbox

Here, we introduce threats faced by information processing (as shown in Fig. 5), the corresponding information security

objectives and classical cryptographic techniques to tackle such threats [50]. First, eavesdropping, which threatens the confidentiality of information, can be prevented using symmetric cryptography and asymmetric cryptography (i.e., public-key cryptography). Second, tampering, which destroys the integrity of data, can be approached with a one-way hash function, message authentication code and digital signatures. Third, disguise, in which the attacker pretends to be the real information sender, can deal with message authentication codes and digital signatures. Finally, one may repudiate his or her certain behavior, and the digital signatures provide the efficacy of nonrepudiation.

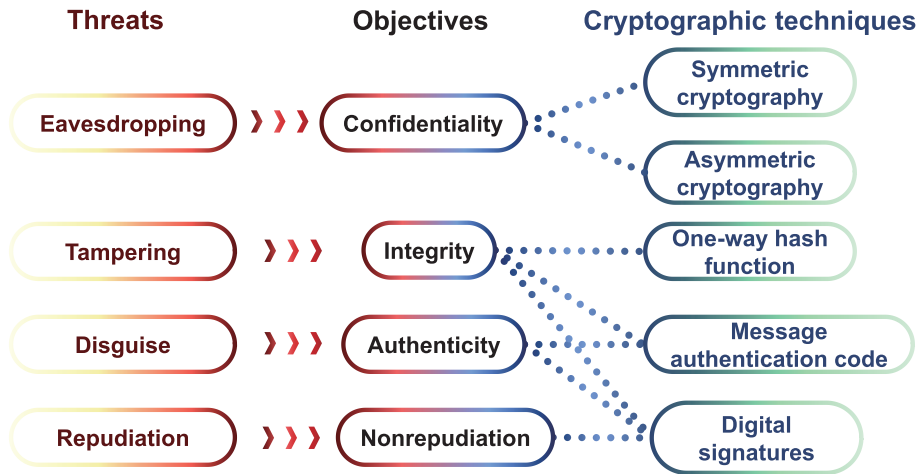


FIG. 5: Cryptography toolbox.

2. One-time pad

Define that encryption algorithm E maps plaintexts $m \in M$ to ciphertexts $c \in C$. According to Shannon's information theory, an algorithm E is perfectly secret if C and M are independent, i.e., $\Pr(m, c) = \Pr(m) \times \Pr(c)$. The one-time pad [12] encryption satisfies the above definition, where a plaintext is paired using the XOR operation with a random secret key of the same length. Learning the ciphertext does not increase any plaintext information. In addition, each encryption requires a new and independent random key; hence, knowing details about the previous key does not help the attacker. In our QDS scheme, we utilize the one-time pad to encrypt the hash value and the irreducible polynomial to acquire the signature so that we can completely conceal the information of hash functions.

3. One-time LFSR-based Toeplitz hashing

A collection H of hash functions $h: \{1, \dots, M\} \rightarrow \{0, \dots, m-1\}$ is said to be universal₂ [51] if for every two different $x, y \in \{1, \dots, M\}$, we have

$$\Pr_{h \in H}[h(x) = h(y)] \leq \frac{1}{m}. \quad (1)$$

The random matrices in H are the universal₂ hash functions, which require mn random bits for specifying hash functions (seen as an mn Boolean matrix) to transform the m -bit document into an n -bit hash value. To reduce the cost of random bits, the Toeplitz matrix, which requires only $n+m-1$ random bits, is now widely used. Nevertheless, it still requires the length of random input bits to be longer than that of the document.

The LFSR-based Toeplitz matrix [45] is the almost universal₂ hash function, where the hash function is determined by an irreducible polynomial $p(x)$ of degree n over Galois field $\text{GF}(2)$ and n -bit input random bits, just requiring a total of $2n$ bits. The randomness of the input string and $p(x)$ together guarantees the security of LFSR-based Toeplitz hashing, and the security bound is $\epsilon = m/2^{n-1}$. In realistic setups, a crucial point is that in every round, the user must randomly choose an irreducible polynomial. In our protocol, Alice finishes this task with an n -bit random number. Denote the format of the irreducible polynomial as $p(x) = x^n + a_{n-1}x^{n-1} + \dots + a_1x + a_0$, where $a_i = 0$ or 1 . Then $p(x)$ can be characterized by an n -bit string $(a_{n-1}, a_{n-2}, \dots, a_1, a_0)$, i.e., every bit of the string determines a corresponding coefficient of $p(x)$. To generate the irreducible polynomial, Alice first uses the n -bit random number to generate a polynomial $p_1(x)$, and checks out whether $p_1(x)$ is irreducible. If $p_1(x)$ is irreducible, it will be used to generate the LFSR-based Toeplitz matrix. Otherwise, Alice utilizes a new n -bit random number to obtain a new string and generates a new polynomial and then examines whether it is an irreducible polynomial. Alice will repeat this step until she generates an irreducible polynomial. For example, choose $n = 128$. Assume Alice first generates $p_1(x) = x^{128} + x^{29} + x^{25} + x + 1$. Then, she will find it reducible and successively generate and examine

$p_2(x) = x^{128} + x^{50} + x^{27} + x^2 + 1$, $p_3(x) = x^{128} + x^{29} + x^{27} + x^2 + 1$. Finally, she finds $p_3(x)$ irreducible and chooses $p_3(x)$ as the irreducible polynomial to generate the Toeplitz matrix. Note that for an irreducible polynomial $p(x)$, one always has $a_0 = 1$. Thus, we can use $n - 1$ random bits $(a_{n-1}, a_{n-2}, \dots, a_1, 1)$ to generate the polynomial. We remark that the random number used for generating the irreducible polynomial is produced locally by Alice.

In the authentication scheme [16, 46], the input random bits and irreducible polynomial can be fixed in the later rounds after the first successful round. In our QDS protocol, however, the input random bits and irreducible polynomial cannot be fixed and must be randomly updated in every round. In other words, the universal₂ hash function will only be used once and then be updated. Thus, we denote it as one-time universal₂ hashing (OTH).

4. Algorithms for testing irreducibility of polynomials over GF(2)

The following is the concrete method we employed to check whether a polynomial over GF(2) is irreducible or not. Suppose $p(x)$ is a polynomial of order n in GF(2). According to [52], the necessary and sufficient condition for $p(x)$ being irreducible is:

$$\begin{cases} (A) x^{2^n} \equiv x \pmod{p(x)} \\ (B) \text{gcf}(x^{2^{\frac{n}{d}}} - x, p(x)) = 1, \end{cases} \quad (2)$$

where d is any prime factor of n , $\text{gcf}(f(x), g(x))$ represents the greatest common factor (GCF) of $f(x)$ and $g(x)$. In our scheme, $n = 128 = 2^7$, i.e., n only has one prime factor “2”. Thus, to verify condition (2), we just need to examine $\text{gcf}(x^{2^{64}} - x, p(x)) = 1$.

To speed up our calculation, we utilize fast modular composition (FMC) algorithms and an extended Euclidean algorithm [53]. The FMC algorithms can calculate $x^{2^{128}}$ and $x^{2^{64}} \pmod{p(x)}$ with high speed by calculating $x^{2^{27}}$ and $x^{2^{26}}$, while the extended Euclidean algorithm can quickly finish the GCF calculation. Thus, conditions (A) and (B) can be verified efficiently. In our simulation we search 1000 irreducible polynomials, and on average, it takes 73.6 tests to find an irreducible polynomial, consistent with the conclusion [45] that the total number of irreducible polynomials of order n in GF(2) is at least $2^{n-1}/n$ and at most $2^n/n$ [2]. We implement our simulation in a desktop with an Intel i5-10400 CPU (with RAM of 8 GB), and on average it takes approximately 0.36 seconds to generate an irreducible polynomial of order 128 from a 128-bit random input.

5. Security analysis

The key bit strings of Alice, Bob and Charlie will have the correlation of secret sharing either Alice makes an XOR operation on two strings of key obtained using quantum key distribution [35–39] or they directly carry out quantum secret sharing [40–44].

Repudiation. Successful repudiation means that Alice wishes that Bob would accept the document while Charlie rejects it. For Alice’s repudiation attacks, Bob and Charlie are both honest and symmetric and they have the same new key strings. They will make the same decision for the same document and signature. In other words, when Bob rejects (accepts) the document, Charlie also rejects (accepts) it. Therefore, our QDS protocol is naturally immune to repudiation.

Forgery. Bob forges successfully when Charlie accepts the forged document forwarded by Bob. According to our protocol, Charlie accepts the message if and only if Charlie obtains the same result through one-time pad encryption and one-time universal₂ hash functions. Since the signature is encrypted by a one-time pad and each hash function is utilized only one time, Bob does not have any information about the used hash function and the generated digest by Alice. Therefore, the probability of a successful forgery can be determined by

$$\epsilon_{\text{for}} = \frac{m}{2^{n-1}}, \quad (3)$$

which is the failure probability of one-time LFSR-based Toeplitz hashing, i.e., one finds two distinct documents to have the identical hash value.

6. Numerical simulation of our QDS via quantum key distribution element

Considering the case that we have two quantum key distribution links between Alice-Bob and Alice-Charlie, the two links have the same loss. Alice and Bob share one set of secret keys S_1 , while Alice and Charlie share the other set of secret keys S_2 by implementing quantum key distribution (QKD) with the key rate R_{QKD} . For the requirement of secret sharing, Alice, Bob and Charlie utilize K_a , K_b and K_c as their correlation keys, respectively, where $K_a = S_1 \oplus S_2$, $K_b = S_1$ and $K_c = S_2$. Therefore, the signature rate can be defined as $R_{\text{QDS}} = R_{\text{QKD}}/3n$, since one needs a $3n$ -bit key to implement OTH and OTP in our QDS protocol.

(6.1) *Sending-or-not-sending twin-field quantum key distribution [35].*

The secure key rate is given by

$$R_{\text{QKD}} = 2t(1-t)\mu e^{-\mu} Y_1 \left[1 - H\left(e_1^{\text{ph}}\right) \right] - Q_Z f H(E^Z), \quad (4)$$

where ϵ is the probability of sending the signal pulse at a signal window, μ is the intensity of the signal pulse, Y_1 is the counting rate of Z_1 -windows, Q_Z is the observed counting rate of Z -windows, $e_1^{\text{ph}} = e_1^{X_1}$ is the phase-flip error rate for Z_1 -windows, E^Z is the bit error rate for Z -windows, and f is the error correction efficiency. The yield Y_1 and error rate $e_1^{X_1}$ can be estimated by exploiting the decoy-state method,

$$Y_1 \geq \frac{\mu/2}{\mu\nu - \nu^2} \left[e^\nu (Q_{\nu 0} + Q_{0\nu}) - \frac{\nu^2}{\mu^2} e^\mu (Q_{\mu 0} + Q_{0\mu}) - 2 \frac{\mu^2 - \nu^2}{\mu^2} Q_{00} \right], \quad (5)$$

$$e_1^{X_1} \leq \frac{1}{2\nu Y_1} \left(e^{2\nu} E_{\nu\nu}^{\text{pm}} Q_{\nu\nu}^{\text{pm}} - \frac{1}{2} Y_0 \right), \quad (6)$$

where ν is the intensity of the decoy pulse, Q_{k_a, k_b} is the gain when Alice chooses intensity k_a and Bob chooses intensity k_b ($k_a, k_b \in \{\mu, \nu, 0\}$), $E_{\nu\nu}^{\text{pm}}$ is the bit error rate, $Q_{\nu\nu}^{\text{pm}}$ is the gain of intensity ν for both Alice and Bob after successful postselected phase-matching and $Y_0 = Q_{00}$ is the counting rate of the vacuum state.

The gain Q_{k_a, k_b} can be given as

$$Q_{k_a, k_b} = 2(1-p_d) e^{-\frac{k_a+k_b}{2}\sqrt{\eta}} \left[I_0\left(\sqrt{k_a k_b} \sqrt{\eta}\right) - (1-p_d) e^{-\frac{k_a+k_b}{2}\sqrt{\eta}} \right], \quad (7)$$

where $\eta = \eta_d^2 \times 10^{-\alpha L/10}$ is the total efficiency and η_d , α and L are the detector efficiency, attenuation coefficient and distance, respectively. p_d is the dark count rate, and $I_0(x)$ is the modified Bessel function of the first kind. The gain $Q_{\nu\nu}^{\text{pm}}$ and bit error rate $E_{\nu\nu}^{\text{pm}}$ can be given by

$$Q_{\nu\nu}^{\text{pm}} = Q_{c,\nu\nu}^{\text{pm}} + Q_{e,\nu\nu}^{\text{pm}}, \quad (8)$$

$$E_{\nu\nu}^{\text{pm}} = [e_d^x Q_{c,\nu\nu}^{\text{pm}} + (1-e_d^x) Q_{e,\nu\nu}^{\text{pm}}] / Q_{\nu\nu}^{\text{pm}}, \quad (9)$$

where e_d^x is the misalignment rate of the X basis. Therein, the correct gain $Q_{c,\nu\nu}^{\text{pm}}$ and incorrect gain $Q_{e,\nu\nu}^{\text{pm}}$ are

$$Q_{c,\nu\nu}^{\text{pm}} \approx \frac{1-p_d}{\delta} \sqrt{\frac{\pi}{2\nu\sqrt{\eta}}} \operatorname{erf}\left(\sqrt{\frac{\nu\sqrt{\eta}}{2}}\delta\right) - (1-p_d)^2 e^{-2\nu\sqrt{\eta}}, \quad (10)$$

$$Q_{e,\nu\nu}^{\text{pm}} \approx \frac{1-p_d}{\delta} e^{-2\nu\sqrt{\eta}} \sqrt{\frac{\pi}{2\nu\sqrt{\eta}}} \operatorname{erfi}\left(\sqrt{\frac{\nu\sqrt{\eta}}{2}}\delta\right) - (1-p_d)^2 e^{-2\nu\sqrt{\eta}}, \quad (11)$$

where $\operatorname{erf}(x)$ and $\operatorname{erfi}(x)$ are the error function and imaginary error function, respectively. The gain Q_Z and bit error rate E^Z can be given by

$$Q_Z = (1-t)^2 Q_{00} + 2t(1-t)Q_{0\mu} + t^2 Q_{\mu\mu}, \quad (12)$$

and

$$E^Z = \frac{(1-t)^2 Q_{00} + t^2 Q_{\mu\mu}}{(1-t)^2 Q_{00} + t(1-t)(Q_{0\mu} + Q_{\mu 0}) + t^2 Q_{\mu\mu}}. \quad (13)$$

In the simulation, we set $p_d = 10^{-8}$, $f = 1.1$, $\eta_d = 85\%$, $e_d = 2\%$ and $\alpha = 0.167$ dB/km. The light intensities and probability t are globally optimized.

(6.2) *Phase-matching quantum key distribution [36].*

Here we present the simulation details of the phase-matching quantum key distribution. The overall secure key rate is given by

$$R_{\text{QKD}} = \frac{2}{D} Q_\mu [1 - h(E^{\text{ph}}) - fh(E^{\text{b}})], \quad (14)$$

where Q_μ is the total gain of the signal pulses, $2/D$ is the phase-sifting factor with $D = 16$, f is the error correction efficiency, $h(x) = -x \log_2 x - (1-x) \log_2 (1-x)$ is the binary entropy function, E^{ph} is the phase error rate and E^{b} is the bit error rate. The overall phase-error rate [54] is bounded by $E^{\text{ph}} \leq 1 - q_1$, where $q_1 = \mu e^{-\mu} Y_1 / Q_\mu$. By using the decoy state method with three intensities, the yield of the single-photon component can be given as

$$Y_1 \geq \frac{\mu}{\mu\nu - \nu^2} \left(Q_\nu e^\nu - Q_\mu e^\mu \frac{\nu^2}{\mu^2} - \frac{\mu^2 - \nu^2}{\mu^2} Q_0 \right). \quad (15)$$

For simulation, the gain of intensity k ($k \in \{\mu, \nu, 0\}$) is $Q_k = 1 - (1 - 2p_d)e^{-k\eta}$. The bit error rate is $E^{\text{b}} = [p_d + \eta\mu(e_\Delta + e_d)] \frac{e^{-\eta\mu}}{Q_\mu}$, where p_d is the dark count rate, $\eta = \eta_d \times 10^{-\alpha L/20}$ is the channel transmittance, e_d is the extra misalignment error and the intrinsic error $e_\Delta = \sin^2(\frac{\pi}{D})$. In the simulation, we set $p_d = 10^{-8}$, $f = 1.1$, $\eta_d = 85\%$, $\alpha = 0.167$ dB/km and $e_d = 2\%$. The intensities μ, ν are globally optimized.

(6.3) Discrete-modulated continuous-variable quantum key distribution [37].

In the case of reverse reconciliation, the secret key rate under collective attacks in the asymptotic limit is given by $R_{\text{QKD}} = p_{\text{pass}} [I(X; Z) - \max_{\rho \in \mathbf{S}} \chi(Z : E)]$, where $I(X; Z)$ is the classical mutual information between Alice's string X and the raw key string Z , $\chi(Z : E)$ is the information of Eve's knowledge about the raw key string Z and $p_{\text{pass}} = 1 - \frac{1}{2} \int_{-\Delta_c}^{\Delta_c} P(q|0) dq - \frac{1}{2} \int_{-\Delta_c}^{\Delta_c} P(q|1) dq$ is the sifting probability. $P(q|0)$ and $P(q|1)$ are probability distributions of Bob's homodyne detection conditioned that Alice generates bit 0 or 1. The set \mathbf{S} contains all density operators compatible with experimental observations. According to [37], this key rate can be reformulated as a convex optimization problem, and the secret key rate is $R = \min_{\rho \in \mathbf{S}} D(\mathcal{G}(\rho) || \mathcal{Z}[\mathcal{G}(\rho)]) - p_{\text{pass}} \delta_{\text{EC}}$, where $D(\rho || \sigma) = \text{Tr}(\rho \log_2 \rho) - \text{Tr}(\rho \log_2 \sigma)$ is the quantum relative entropy. \mathcal{G} is a map describing classical postprocessing. For the reverse reconciliation, we have $\mathcal{G}(\sigma) = K \sigma K^\dagger$, where $K = \sum_{z=0}^1 |z\rangle_R \otimes (|0\rangle\langle 0| + |1\rangle\langle 1|)_A \otimes (\sqrt{I_z})_B$ with $I_0 = \int_{\Delta_c}^{\infty} dq |q\rangle\langle q|$ and $I_1 = \int_{-\infty}^{-\Delta_c} dq |q\rangle\langle q|$. We set $\Delta_c = 0$ in our simulation. \mathcal{Z} is a pinching quantum channel, and we have $\mathcal{Z}(\rho) = \sum_j Z_j \rho Z_j$, where $Z_0 = |0\rangle\langle 0|_R \otimes \mathcal{I}_{AB}$ and $Z_1 = |1\rangle\langle 1|_R \otimes \mathcal{I}_{AB}$. $\delta_{\text{EC}} = (1 - \beta)H(Z) + \beta h(e)$ is the amount of information leakage per signal, where $e = \frac{1}{p_{\text{pass}}} \left(\frac{1}{2} \int_{-\infty}^{-\Delta_c} P(q|0) dq + \frac{1}{2} \int_{\Delta_c}^{\infty} P(q|1) dq \right)$. The convex optimization problem can be described as follows:

$$\begin{aligned} & \text{minimize} \quad D(\mathcal{G}(\rho) || \mathcal{Z}[\mathcal{G}(\rho)]) \\ & \text{subject to} \\ & \quad \text{Tr}[\rho(|i\rangle\langle i|_A \otimes \hat{q})] = p_x \langle \hat{q} \rangle_i, \\ & \quad \text{Tr}[\rho(|i\rangle\langle i|_A \otimes \hat{p})] = p_x \langle \hat{p} \rangle_i, \\ & \quad \text{Tr}[\rho(|i\rangle\langle i|_A \otimes \hat{n})] = p_x \langle \hat{n} \rangle_i, \\ & \quad \text{Tr}[\rho(|i\rangle\langle i|_A \otimes \hat{d})] = p_x \langle \hat{d} \rangle_i, \\ & \quad \text{Tr}[\rho] = 1, \\ & \quad \rho \geq 0, \\ & \quad \text{Tr}_B[\rho] = \sum_{i,j=0}^3 \sqrt{p_i p_j} \langle \phi_j | \phi_i \rangle |i\rangle\langle j|_A, \end{aligned} \quad (16)$$

where $\hat{n} = \frac{1}{2}(\hat{q}^2 + \hat{p}^2 - 1) = \hat{a}^\dagger \hat{a}$ and $\hat{d} = \hat{q}^2 - \hat{p}^2 = \hat{a}^2 + (\hat{a}^\dagger)^2$. We consider a quantum channel with transmittance $\eta = 10^{-0.167L/10}$ where L is the distance and excess noise $\xi = 0.01$. In such a model, we have $P(q|0) = \frac{1}{\sqrt{\pi(1+\eta\xi)}} e^{-\frac{[\alpha - \sqrt{2\eta}q]^2}{1+\eta\xi}}$ and $P(q|1) = \frac{1}{\sqrt{\pi(1+\eta\xi)}} e^{-\frac{[\alpha + \sqrt{2\eta}q]^2}{1+\eta\xi}}$. The expectation values can be given by

$$\begin{aligned} \langle \hat{q} \rangle &= \sqrt{2\eta} \text{Re}(\alpha), \\ \langle \hat{p} \rangle &= \sqrt{2\eta} \text{Im}(\alpha), \\ \langle \hat{n} \rangle &= \eta |\alpha|^2 + \frac{\eta\xi}{2}, \\ \langle \hat{d} \rangle &= \eta [\alpha^2 + (\alpha^*)^2]. \end{aligned} \quad (17)$$

α is the amplitude of the signal, and we optimize α in the interval of $[0.35, 0.6]$ with a step of 0.01.

(6.4) *Gaussian-modulated continuous-variable quantum key distribution [38].*

From an information-theoretic point of view, in the case of reverse reconciliation, Alice and Bob can distill perfectly correlated secret key bits provided that the amount of information they share I_{AB} is higher than the information acquired by Eve χ_{BE} under collective attacks. Therefore, the secret key rate is defined as $R = I_{AB} - \chi_{AB}$. Considering the inefficiency of error correction, a factor β is introduced as the reconciliation efficiency, and the secret key rate formula is $R_{\text{QKD}} = \beta I_{AB} - \chi_{AB}$. In our numerical simulation, we use $\beta = 0.95$. We calculate the mutual information using

$$I_{AB} = \frac{1}{2} \log_2 \frac{V + \chi_{\text{tot}}}{1 + \chi_{\text{tot}}}, \quad (18)$$

where V is the variance of the thermal state observed at Alice's lab, and χ_{tot} is the total excess noise added between Alice and Bob. Here, we detail the formula of χ_{tot} as follows:

$$\chi_{\text{tot}} = \frac{1}{\eta T(1 + v_{\text{el}}) + \xi - 1}, \quad (19)$$

where T is the transmission of the quantum channel, ξ is the excess noise, v_{el} is the electronic noise and η is the detection losses. To draw the line, we set $\eta = 0.85$, $v_{\text{el}} = 0$, $\xi = 0.01$, $T = 10^{-0.167L/10}$ and V is optimized. L is the distance. Under collective attacks, Eve's accessible information is upper bounded by the Holevo quantity χ_{BE} satisfying

$$\chi_{BE} = G\left(\frac{\lambda_1 - 1}{2}\right) + G\left(\frac{\lambda_2 - 1}{2}\right) - G\left(\frac{\lambda_3 - 1}{2}\right) - G\left(\frac{\lambda_4 - 1}{2}\right), \quad (20)$$

where $G(x) = (x+1)\log_2(x+1) - x\log_2 x$, and $\{\lambda_i\}$ are the symplectic eigenvalues of the covariance matrix characterizing the quantum state. Calculation shows that $\lambda_{1,2}^2 = \frac{1}{2}[A \pm \sqrt{A^2 - 4B}]$, where $A = V^2(1-2T) + 2T + T^2(V + \xi - 1 + \frac{1}{T})^2$ and $B = T^2(V/T - V + V\xi + 1)^2$ and $\lambda_{1,2}^2 = \frac{1}{2}[C \pm \sqrt{C^2 - 4D}]$, where $C = \frac{V\sqrt{B} + T(V+1/T-1+\xi) + A/\eta(1+v_{\text{el}}) - A}{T(V+\chi_{\text{tot}})}$ and $D = \sqrt{B} \frac{V + \sqrt{B}[1/\eta(1+v_{\text{el}}) - 1]}{T(V+\chi_{\text{tot}})}$.

(6.5) *Measurement-device-independent quantum key distribution [39].*

For the measurement-device-independent quantum key distribution, we consider Alice and Bob sending a coherent state and the ideal case where only the channel loss and detector efficiency are taken into consideration. The secret key rate is given by

$$R_{\text{QKD}} = \frac{1}{2e^2} \eta^2, \quad (21)$$

where $\eta = \eta_d \times 10^{-\alpha L/20}$ is the total channel transmittance and L is the distance between Alice and Bob. We set $\eta_d = 85\%$, $\alpha = 0.167$ dB/km.

7. Numerical simulation of our QDS via quantum secret sharing element

Different from quantum key distribution, quantum secret sharing can directly offer secret sharing correlation with unconditional security via quantum laws. In quantum secret sharing of three users, Alice is the dealer, while both Bob and Charlie are players. Even though one of Bob and Charlie is dishonest, they can also generate the secure correlation key $K_a = K_b \oplus K_c$. We assume that the distances of Alice-Bob and Alice-Charlie are the same. The signature rate can be defined as $R_{\text{QDS}} = R_{\text{QSS}}/3n$, since one needs a $3n$ -bit key for OTH and OTP.

(7.1) *Prepare-and-measure quantum secret sharing [40].*

Using the Greenberger-Horne-Zeilinger (GHZ) state can realize quantum secret sharing directly. Here, we consider an equivalent prepare-and-measure protocol. In our simulation, we only consider the photon loss in the quantum channel and detector. Therefore, the secret key rate is given by

$$R_{\text{QSS}} = \eta^2, \quad (22)$$

where $\eta = \eta_d \times 10^{-\alpha L/10}$, $\eta_d = 85\%$ and $\alpha = 0.167$ dB/km. L is the distance between Alice and Bob (Charlie).

(7.2) *Measurement-device-independent quantum secret sharing [41].*

By exploiting the postselected GHZ state, one can also realize quantum secret sharing. We only consider the photon loss from quantum channels and detectors here. The secret key rate of using a single-photon source can be given by

$$R_{\text{QSS}} = \frac{1}{4}\eta_d\eta^2. \quad (23)$$

Here, we have $\eta = \eta_d \times 10^{-\alpha L/10}$, $\eta_d = 85\%$, $\alpha = 0.167$ dB/km and assume that there is no loss of Alice's photon. The factor 1/4 comes from only two of eight GHZ states that can be identified. L is the distance between Alice and Bob (Charlie).

(7.3) *Round-robin quantum secret sharing [42].*

The secret key rate per pulse of the round-robin quantum secret sharing with a twin-field for sending d coherent pulses each train in the case of the inside adversary can be written as

$$R_{\text{QSS}} = \frac{1}{d}\{\hat{Q}[1 - h(\hat{e}_p)] - Qfh(e_b)\}, \quad (24)$$

where we have $\hat{Q} = \min\{Q_A, Q_B\}$. Q_A and Q_B are the gains of Charlie's successful detection from Alice and Bob, respectively. The phase error rate is

$$\hat{e}_p = \frac{e_{\text{src}}}{\hat{Q}} + \left(1 - \frac{e_{\text{src}}}{\hat{Q}}\right) \frac{n_{\text{th}}}{d-1}. \quad (25)$$

The average gain Q and bit error rate e_b of each train can be written as

$$Q = \frac{1}{2}[1 - (1 - dp_d)e^{-2\mu\eta}], \quad (26)$$

and

$$e_b = \frac{e_d(1 - e^{-2\mu\eta}) + dp_de^{-2\mu\eta}/2}{1 - (1 - dp_d)e^{-2\mu\eta}}, \quad (27)$$

where $\eta = \eta_d \times 10^{-\alpha L/10}$ is the efficiency between Alice and Bob (Charlie). In addition, we have the gains $Q_A = Q_B = Q/2$ due to the symmetry. Let n be the total photon number in a train of optical pulses with total intensity μ . Then, the probability of finding more than n_{th} photons in a train of optical pulses can be written as

$$\Pr(n > n_{\text{th}}) = e_{\text{src}} := 1 - \sum_{n=0}^{n_{\text{th}}} \frac{e^{-\mu}\mu^n}{n!}, \quad (28)$$

where n_{th} is an integer constant chosen in this protocol. For the simulation, we set $p_d = 10^{-8}$, $f = 1.1$, $\eta_d = 85\%$, $\alpha = 0.167$ dB/km and $e_d = 2\%$. The intensity μ , the selected integer n_{th} and the number of optical pulses d are globally optimized.

(7.4) *Single-qubit quantum secret sharing [43].*

For the single-qubit quantum secret sharing protocol with a single photon source, the final key rate can be easily derived based on phase-error correction

$$R_{\text{QSS}} = Q_1[1 - h(e_p) - fh(e_b)], \quad (29)$$

where $e_p = e_b = p_d(1 - 2e_d)/Q_1 + e_d$ and $Q_1 = \mu e^{-\mu}(2p_d + \eta - 2p_d\eta)$. $\eta = \eta_d \times 10^{-\alpha \cdot 2L/10}$ is the total transmittance; $2L$ is the total distance. The intensity μ is globally optimized. We set $p_d = 10^{-8}$, $f = 1.1$, $\eta_d = 85\%$, $\alpha = 0.167$ dB/km and $e_d = 2\%$.

(7.5) *Differential-phase-shift quantum secret sharing [44].*

The final key rate for differential-phase-shift quantum secret sharing using a twin-field is bounded by

$$R_{\text{QSS}} = Q_\mu[-(1 - 2\mu)\log_2(P_{\text{co}}) - fh(E_\mu)], \quad (30)$$

TABLE II: List of the experimental data used for one-time secure key generation.

	Alice-Bob (101 km)	Alice-Charlie (126 km)
n_μ^z	4616266	5225387
n_ν^z	258671	296285
n_ω^z	394425	437496
n_0^z	11189	14080
n_μ^x	1035046	1311484
n_ν^x	58107	78890
n_ω^x	87317	110362
n_0^x	3126	8168
m_ω^z	3446	9401

where Q_μ is the gain of the whole system. $h(x) = -x \log_2(x) - (1-x) \log_2(1-x)$ is the Shannon entropy, and f is the error correction efficiency. P_{co} is the upper bound of collision probability when considering individual attacks, which can be concluded as $P_{\text{co}} = 1 - E_\mu^2 - (1 - 6E_\mu)^2/2$. The total gain and the total error rate with an intensity of μ are given by

$$\begin{aligned} Q_\mu &= 1 - (1 - 2p_d)e^{-\mu\eta}, \\ E_\mu Q_\mu &= e_d Q_\mu + \left(\frac{1}{2} - e_d\right) 2p_d e^{-\mu\eta}, \end{aligned} \quad (31)$$

where e_d is the misalignment error rate of detectors. $\eta = \eta_d \times 10^{-\alpha L/10}$ is the efficiency between Alice and Bob (Charlie), where η_d is the detection efficiency of Charlie's detectors. The intensity is globally optimized. We set $p_d = 10^{-8}$, $f = 1.16$, $\eta_d = 85\%$, $\alpha = 0.167$ dB/km and $e_d = 2\%$.

8. Experimental details

In the transmitting end, a master laser generates a repetition rate of 200 MHz and phase-randomized laser pulses 1.6 ns-wide at 1550.12 nm. An asymmetric interferometer with a 2 ns time delay divides each master pulse into two pairs of optical pulses with relative phases 0 and π . Then, the two pairs of optical pulses are injected into two slave lasers through the optical circulator. With the help of controlling the trigger electrical signal of two slave lasers, one generates a quantum signal only in the first time-bin or the second time-bin to constitute the Z basis, and one prepares a quantum signal both in two time-bins with a 0 or π phase difference to constitute the X basis. A 50 GHz bandwidth fiber Bragg grating is exploited to precompensate for pulse broadening and to remove extra spurious emission. The 2 ns-wide synchronization pulses with repetition rates of 100 kHz are transmitted via the quantum channel by using wavelength division multiplexed. The slave pulse width is 400 ps, which is much larger than the 10 ps timing resolution of the programmable delay chip, which means that the time consistency can be accurately calibrated. The spectral consistency is naturally satisfied through the laser seeding technique [55].

In the receiving end, a 30:70 biased beam splitter is used to perform passive basis detection after a wavelength division demultiplexer. A probability of 30% is measured in phase interference and the probability of 70% is used to receive in the time basis. A Faraday-Michelson interferometer realizes the phase measurement, where phase drift is compensated in real time by using the phase shifter. The total insertion losses of the time and phase bases are 4.25 and 8 dB, respectively. The efficiency of single-photon detectors is 20% at a 160 dark count per second. To decrease the after-pulse probability, we set the dead times to 10 and 25 μs for the Bob-Alice and Charlie-Alice links, respectively.

A four-intensity decoy-state protocol [56–58] is adopted, where the intensities of the Z basis are set as $\mu = 0.35$ and $\nu = 0.15$, and the intensity of the X basis is $\omega = 0.3$. The intensity of the vacuum state is 0, which does not contain any basis information. The corresponding probabilities are $p_\mu = 0.78$, $p_\nu = 0.1$, $p_\omega = 0.08$ and $p_0 = 0.04$. Thereinto, the amplitude modulator generates two different intensities, and the intensity of ω is double that of ν since it has two pulses in the X basis.

The error correction and privacy amplification are carried out using a field-programmable gate array. Each time, privacy amplification will be performed after accumulating data approximately to the size of 4 Mb via approximately ten times of error correction, where the data size excludes the amount of information leaked in error correction. For the link of Alice-Bob with 101 km (Alice-Charlie with 126 km), one needs to accumulate approximately 153 (560) seconds of data for privacy amplification to extract a secure key. Here, we only list the experimental data of one set and calculation results related to privacy amplification, as shown in Tables I and II.

TABLE III: List of the calculation results used for one-time secure key generation.

	Alice-Bob (101 km)	Alice-Charlie (126 km)
R_{QKD} (bps)	6021	470
Λ (s)	152.8	561
\underline{s}_0^{zz}	159429	203152
\underline{s}_1^{zz}	2756924	3158726
λ_{EC}	1225992	1659948
ℓ	920042	263482
$\bar{\phi}_1^{zz}$	4.83%	9.57%
ε_{sec}	10^{-10}	10^{-10}

TABLE IV: Simulation parameters of the link between Alice-Bob (Charlie). e_d^z and e_d^x are the misalignment rates of the Z and X bases, and t_{dead} is the dead time of the detector.

Clock frequency	η_d	p_d	e_d^z	e_d^x	t_{dead}	ε_{cor}	f
2×10^8	20%	0.8×10^{-6}	2.3% (2.2%)	1.9% (2.4%)	10 (25) μs	10^{-15}	1.42

To compare with the experimental results, we use the relevant experimental parameters to simulate the secure key rate, as shown in Table III. The length of the final key, which is ε_{cor} -correct and ε_{sec} -secret, can be given by [49, 59]

$$\ell = \underline{s}_0^{zz} + \underline{s}_1^{zz} \left[1 - h\left(\bar{\phi}_1^{zz}\right) \right] - \lambda_{\text{EC}} - \log_2 \frac{2}{\varepsilon_{\text{cor}}} - 6 \log_2 \frac{22}{\varepsilon_{\text{sec}}}, \quad (32)$$

where $h(x) := -x \log_2 x - (1-x) \log_2 (1-x)$, and \bar{x} (\underline{x}) denotes the upper (lower) bound of the observed value x . Using the decoy-state method for finite sample sizes, the expected numbers of vacuum events \underline{s}_0^{zz*} and single-photon events \underline{s}_1^{zz*} can be written as

$$\underline{s}_0^{zz*} \geq (e^{-\mu} p_\mu + e^{-\nu} p_\nu) \frac{\bar{n}_0^{zz*}}{p_0}, \quad (33)$$

and

$$\underline{s}_1^{zz*} \geq \frac{\mu^2 e^{-\mu} p_\mu + \mu \nu e^{-\nu} p_\nu}{\mu \nu - \nu^2} \times \left(e^\nu \frac{\bar{n}_\nu^{zz*}}{p_\nu} - \frac{\nu^2}{\mu^2} e^\mu \frac{\bar{n}_\mu^{zz*}}{p_\mu} - \frac{\mu^2 - \nu^2}{\mu^2} \frac{\bar{n}_0^{zz*}}{p_0} \right), \quad (34)$$

where $n_k^{z(x)}$ is the count of k ($k \in \{\mu, \nu, \omega\}$) intensity pulse measured in the $Z(X)$ basis, and x^* is the corresponding expected value of given observed value x . The upper and lower bounds can be acquired [60] by using the variant of the Chernoff bound, $\bar{x}^* = x + \beta + \sqrt{2\beta x + \beta^2}$ and $\underline{x}^* = x - \frac{\beta}{2} - \sqrt{2\beta x + \frac{\beta^2}{4}}$, where $\beta = \ln \frac{22}{\varepsilon_{\text{sec}}}$. The expected number of single-photon events \underline{s}_1^{xx*} in \mathcal{X}_ω can be given by [58]

$$\underline{s}_1^{xx*} \geq \frac{\mu \omega e^{-\omega} p_\omega}{\mu \nu - \nu^2} \left(e^\nu \frac{\bar{n}_\nu^{xx*}}{p_\nu} - \frac{\nu^2}{\mu^2} e^\mu \frac{\bar{n}_\mu^{xx*}}{p_\mu} - \frac{\mu^2 - \nu^2}{\mu^2} \frac{\bar{n}_0^{xx*}}{p_0} \right). \quad (35)$$

In addition, the expected number of bit errors t_1^{xx*} associated with the single-photon event in \mathcal{X}_ω is $\bar{t}_1^{xx} \leq m_\omega^x - t_0^{xx}$, with $t_0^{xx} = \frac{e^{-\omega} p_\omega \bar{n}_0^{xx*}}{2p_0}$. For a given expected value, the upper and lower bounds of the observed value can be given as $\bar{x} = x^* + \frac{\beta}{2} + \sqrt{2\beta x^* + \frac{\beta^2}{4}}$ and $\underline{x} = x^* - \sqrt{2\beta x^*}$, respectively. By using random sampling without replacement, the phase error rate in the Z basis is

$$\bar{\phi}_1^{zz} = \frac{\bar{t}_1^{xx}}{\underline{s}_1^{xx}} + \gamma^U \left(\underline{s}_1^{zz}, \underline{s}_1^{xx}, \frac{\bar{t}_1^{xx}}{\underline{s}_1^{xx}}, \frac{\varepsilon_{\text{sec}}}{22} \right), \quad (36)$$

where we have $\gamma^U(n, k, \lambda, \epsilon) = \frac{(1-2\lambda)AG}{n+k} + \sqrt{\frac{A^2 G^2}{(n+k)^2} + 4\lambda(1-\lambda)G}$, with $A = \max\{n, k\}$ and $G = \frac{n+k}{nk} \ln \frac{n+k}{2\pi nk\lambda(1-\lambda)\epsilon^2}$.

Experimental demonstration the single-bit-type QDS of Ref. [24].

All the shared keys do not require error correction, and privacy amplification, i.e., n_μ , can be used for signature. For a one-bit message, suppose that $2L$ bits of keys are used. Then the security level of the signature can be bounded by [31]

$$\epsilon = \max(P(\text{honest abort}), P(\text{repudiation}), P(\text{forge})), \quad (37)$$

$$P(\text{honest abort}) = 2e^{-(s_a - \bar{E})^2 L}, \quad (38)$$

$$P(\text{repudiation}) = 2e^{-(s_v - s_a)^2 L}, \quad (39)$$

$$P(\text{forge}) = 2e^{-(p_e - s_v)^2 L}. \quad (40)$$

where we choose $s_a = \bar{E} + \frac{p_e - \bar{E}}{3}$, $s_v = \bar{E} + \frac{2(p_e - \bar{E})}{3}$, and \bar{E} is the upper bound bit error rate of the signal state. p_e can be determined by

$$\underline{c}_0^{zz} + \underline{c}_1^{zz}[1 - h(\bar{\phi}_1^{zz})] = h(p_e) \quad (41)$$

where $\underline{c}_i^{zz} = \underline{s}_i^{zz}/n_\mu$.

Note that it is different between the Bob-Alice link and Charlie-Alice link. The parameters \bar{E} and p_e should choose the maximal and minimum values, respectively. By using the experimental data, we can estimate $p_e = 7.06\%$, $s_v = 5.79\%$, $s_a = 4.52\%$ and $\bar{E} = 3.24\%$. Thus, to sign one bit, we need raw keys with $2L = 1.09 \times 10^6$ (4.66×10^5) bits, and the probability of honest abort, repudiation and forge are $P(\text{honest abort}) = P(\text{repudiation}) = P(\text{forge}) = \hat{\epsilon} = 10^{-38}$ (10^{-16}), respectively. When the length of the document is one megabit, the signature security bound $\hat{\epsilon} = 10^{-16}$ is $\epsilon = 1 - (1 - \hat{\epsilon}^{10^6}) \approx 10^6 \cdot \hat{\epsilon} = 10^{-32}$ (10^{-10}).

-
- [1] A. Fedorov, E. Kiktenko, and A. Lvovsky, *Nature* **563**, 465 (2018).
 - [2] A. J. Menezes, P. C. Van Oorschot, and S. A. Vanstone, *Handbook of applied cryptography* (2018).
 - [3] X. Wang and H. Yu, *How to break md5 and other hash functions* (2005).
 - [4] X. Wang, Y. L. Yin, and H. Yu, in *Advances in Cryptology - CRYPTO 2005: 25th Annual International Cryptology Conference, Santa Barbara, California, USA, August 14-18, 2005, Proceedings* (2005), vol. 3621 of *Lecture Notes in Computer Science*.
 - [5] M. Stevens, E. Bursztein, P. Karpman, A. Albertini, and Y. Markov, *The first collision for full sha-1* (2017).
 - [6] T. Kleinjung, K. Aoki, J. Franke, A. K. Lenstra, E. Thomé, J. W. Bos, P. Gaudry, A. Kruppa, P. L. Montgomery, D. A. Osvik, et al., in *Advances in Cryptology - CRYPTO 2010* (2010).
 - [7] T. Kleinjung, C. Diem, A. K. Lenstra, C. Priplata, and C. Stahlke, *Computation of a 768-bit prime field discrete logarithm* (2017).
 - [8] F. Boudot, P. Gaudry, A. Guillevic, N. Heninger, E. Thomé, and P. Zimmermann, *Comparing the difficulty of factorization and discrete logarithm: a 240-digit experiment* (2020).
 - [9] R. L. Rivest, A. Shamir, and L. Adleman, *Commun. ACM* **21** (1978).
 - [10] T. ElGamal, *IEEE transactions on information theory* **31**, 469 (1985).
 - [11] P. W. Shor, *Algorithms for quantum computation: discrete logarithms and factoring* (1994).
 - [12] C. E. Shannon, *The Bell System Technical Journal* **27**, 379 (1948).
 - [13] C. H. Bennett and G. Brassard, *Theor. Comput. Sci.* **560**, 7 (2014).
 - [14] B. Fröhlich, J. F. Dynes, M. Lucamarini, A. W. Sharpe, Z. Yuan, and A. J. Shields, *Nature* **501**, 69 (2013).
 - [15] S. Wengerowsky, S. K. Joshi, F. Steinlechner, H. Hübel, and R. Ursin, *Nature* **564**, 225 (2018).
 - [16] Y.-A. Chen, Q. Zhang, T.-Y. Chen, W.-Q. Cai, S.-K. Liao, J. Zhang, K. Chen, J. Yin, J.-G. Ren, Z. Chen, et al., *Nature* **589**, 214 (2021).
 - [17] Z. Qi, Y. Li, Y. Huang, J. Feng, Y. Zheng, and X. Chen, *Light Sci. Appl.* **10**, 183 (2021).
 - [18] Y.-B. Sheng, L. Zhou, and G.-L. Long, *Sci. Bull.* (2022).
 - [19] V. Lyubashevsky, *National Science Review* **8**, nwab077 (2021).
 - [20] D. Gottesman and I. Chuang, *arXiv preprint quant-ph/0105032* (2001).

- [21] P. J. Clarke, R. J. Collins, V. Dunjko, E. Andersson, J. Jeffers, and G. S. Buller, *Nature Commun.* **3**, 1174 (2012).
- [22] V. Dunjko, P. Wallden, and E. Andersson, *Phys. Rev. Lett.* **112**, 040502 (2014).
- [23] H.-L. Yin, Y. Fu, and Z.-B. Chen, *Phys. Rev. A* **93**, 032316 (2016).
- [24] R. Amiri, P. Wallden, A. Kent, and E. Andersson, *Phys. Rev. A* **93**, 032325 (2016).
- [25] Y.-S. Lu, X.-Y. Cao, C.-X. Weng, J. Gu, Y.-M. Xie, M.-G. Zhou, H.-L. Yin, and Z.-B. Chen, *Opt. Express* **29**, 10162 (2021).
- [26] C.-X. Weng, Y.-S. Lu, R.-Q. Gao, Y.-M. Xie, J. Gu, C.-L. Li, B.-H. Li, H.-L. Yin, and Z.-B. Chen, *Opt. Express* **29**, 27661 (2021).
- [27] R. J. Collins, R. J. Donaldson, V. Dunjko, P. Wallden, P. J. Clarke, E. Andersson, J. Jeffers, and G. S. Buller, *Phys. Rev. Lett.* **113**, 040502 (2014).
- [28] H.-L. Yin, Y. Fu, H. Liu, Q.-J. Tang, J. Wang, L.-X. You, W.-J. Zhang, S.-J. Chen, Z. Wang, Q. Zhang, et al., *Phys. Rev. A* **95**, 032334 (2017).
- [29] H.-L. Yin, W.-L. Wang, Y.-L. Tang, Q. Zhao, H. Liu, X.-X. Sun, W.-J. Zhang, H. Li, I. V. Puthoor, L.-X. You, et al., *Phys. Rev. A* **95**, 042338 (2017).
- [30] G. Roberts, M. Lucamarini, Z. Yuan, J. Dynes, L. Comandar, A. Sharpe, A. Shields, M. Curty, I. Puthoor, and E. Andersson, *Nature Commun.* **8**, 1098 (2017).
- [31] X.-B. An, H. Zhang, C.-M. Zhang, W. Chen, S. Wang, Z.-Q. Yin, Q. Wang, D.-Y. He, P.-L. Hao, S.-F. Liu, et al., *Opt. Lett.* **44**, 139 (2019).
- [32] S. Richter, M. Thornton, I. Khan, H. Scott, K. Jaksch, U. Vogl, B. Stiller, G. Leuchs, C. Marquardt, and N. Korolkova, *Phys. Rev. X* **11**, 011038 (2021).
- [33] T.-Y. Wang, X.-Q. Cai, Y.-L. Ren, and R.-L. Zhang, *Sci. Rep.* **5**, 9231 (2015).
- [34] M.-C. Roehsner, J. A. Kettlewell, J. Fitzsimons, and P. Walther, *npj Quantum Inf.* **7**, 98 (2021).
- [35] X.-B. Wang, Z.-W. Yu, and X.-L. Hu, *Phys. Rev. A* **98**, 062323 (2018).
- [36] X. Ma, P. Zeng, and H. Zhou, *Phys. Rev. X* **8**, 031043 (2018).
- [37] J. Lin, T. Upadhyaya, and N. Lütkenhaus, *Phys. Rev. X* **9**, 041064 (2019).
- [38] J. Lodewyck, M. Bloch, R. García-Patrón, S. Fossier, E. Karpov, E. Diamanti, T. Debuisschert, N. J. Cerf, R. Tualle-Broui, S. W. McLaughlin, et al., *Phys. Rev. A* **76**, 042305 (2007).
- [39] H.-K. Lo, M. Curty, and B. Qi, *Phys. Rev. Lett.* **108**, 130503 (2012).
- [40] M. Hillery, V. Bužek, and A. Berthiaume, *Phys. Rev. A* **59**, 1829 (1999).
- [41] Y. Fu, H.-L. Yin, T.-Y. Chen, and Z.-B. Chen, *Phys. Rev. Lett.* **114**, 090501 (2015).
- [42] J. Gu, Y.-M. Xie, W.-B. Liu, Y. Fu, H.-L. Yin, and Z.-B. Chen, *Opt. Express* **29**, 32244 (2021).
- [43] C. Schmid, P. Trojek, M. Bourennane, C. Kurtsiefer, M. Żukowski, and H. Weinfurter, *Phys. Rev. Lett.* **95**, 230505 (2005).
- [44] J. Gu, X.-Y. Cao, H.-L. Yin, and Z.-B. Chen, *Opt. Express* **29**, 9165 (2021).
- [45] H. Krawczyk, in *Annual International Cryptology Conference* (1994), pp. 129–139.
- [46] C.-H. F. Fung, X. Ma, and H. Chau, *Phys. Rev. A* **81**, 012318 (2010).
- [47] S. Wehner, D. Elkouss, and R. Hanson, *Science* **362**, eaam9288 (2018).
- [48] M. Pompili, S. L. N. Hermans, S. Baier, H. K. C. Beukers, P. C. Humphreys, R. N. Schouten, R. F. L. Vermeulen, M. J. Tiggelman, L. dos Santos Martins, B. Dirkse, et al., *Science* **372**, 259 (2021).
- [49] H.-L. Yin, P. Liu, W.-W. Dai, Z.-H. Ci, J. Gu, T. Gao, Q.-W. Wang, and Z.-Y. Shen, *Opt. Express* **28**, 29479 (2020).
- [50] B. Schneier, *Secrets and lies: digital security in a networked world* (John Wiley & Sons, 2015).
- [51] J. L. Carter and M. N. Wegman, *Journal of Computer and System Sciences* **18**, 143 (1979).
- [52] M. O. Rabin, *SIAM Journal on computing* **9**, 273 (1980).
- [53] J. Von Zur Gathen and J. Gerhard, *Modern computer algebra* (Cambridge university press, 2013).
- [54] P. Zeng, W. Wu, and X. Ma, *Phys. Rev. Appl.* **13**, 064013 (2020).
- [55] L. Comandar, M. Lucamarini, B. Fröhlich, J. Dynes, A. Sharpe, S.-B. Tam, Z. Yuan, R. Penty, and A. Shields, *Nat. Photonics* **10**, 312 (2016).
- [56] X.-B. Wang, *Phys. Rev. Lett.* **94**, 230503 (2005).
- [57] H.-K. Lo, X. Ma, and K. Chen, *Phys. Rev. Lett.* **94**, 230504 (2005).
- [58] Z.-W. Yu, Y.-H. Zhou, and X.-B. Wang, *Phys. Rev. A* **93**, 032307 (2016).
- [59] C. C. W. Lim, M. Curty, N. Walenta, F. Xu, and H. Zbinden, *Phys. Rev. A* **89**, 022307 (2014).
- [60] H.-L. Yin, M.-G. Zhou, J. Gu, Y.-M. Xie, Y.-S. Lu, and Z.-B. Chen, *Sci. Rep.* **10**, 14312 (2020).